Letter

Universal scaling for the permeability of random packs of overlapping and nonoverlapping particles

Jérémie Vasseur,[1,*] Fabian B. Wadsworth,[2] Eloïse Bretagne,[2] and Donald B. Dingwell[1]
[1]*Earth and Environmental Science, Ludwig-Maximilians-Universität, Theresienstrasse 41, 80333 Munich, Germany*
[2]*Department of Earth Sciences, Science Laboratories, Durham University, Durham DL1 3LE, United Kingdom*

(Received 12 January 2022; accepted 8 March 2022; published 20 April 2022)

Constraining fluid permeability in porous media is central to a wide range of theoretical, industrial, and natural processes. In this Letter, we validate a scaling for fluid permeability in random and lattice packs of spheres and show that the permeability of packs of both hard and overlapping spheres of any sphere size or size distribution collapse to a universal curve across all porosity ϕ in the range of $\phi_c < \phi < 1$, where ϕ_c is the percolation threshold. We use this universality to demonstrate that permeability can be predicted using percolation theory at $\phi_c < \phi \lesssim 0.30$, Kozeny-Carman models at $0.30 \lesssim \phi \lesssim 0.40$, and dilute expansions of Stokes theory for lattice models at $\phi \gtrsim 0.40$. This result leads us to conclude that the inverse specific surface area, rather than an effective sphere size or pore size is a universal controlling length scale for hydraulic properties of packs of spheres. Finally, we extend this result to predict the permeability for some packs of concave nonspherical particles.

DOI: 10.1103/PhysRevE.105.L043301

The hydraulic properties of porous media are controlled by their internal microstructure [1]. In particular, the permeability depends on the distribution, geometry, and scale of the internal porous channel pathways [2]. Thus, a central goal of material research is to find simple relationships between macroscopic properties, such as fluid permeability and the measurable characteristics of microstructure [1–7]. To date, many different such relationships have been proposed possessing variable degrees of freedom in the form of parameters that can be adjusted in order to accurately capture the permeability of a given system [2,5,8–12]. Yet in one of the seemingly simplest such systems, composed of spherical objects packed in a volume, there is no clear framework for bringing together and comparing data across the entire range of microstructural characteristics and sphere size distributions. Here, we formulate and test a framework for comparing systems of spheres for which the spheres can and cannot overlap with one another, and systems in which the spheres are a continuous distribution of radii.

The slow flow of viscous and incompressible fluids through porous media is given by Darcy's law, which relates the pressure gradient ∇p driving flow with the resultant fluid filtration velocity u via the dynamic fluid viscosity μ and the permeability k of the porous medium and is [13,14]

$$u = -\frac{k}{\mu}\nabla p, \tag{1}$$

where k depends on the volume fraction of the pore space ϕ. An area of broad interest is to find rigorous models for $k(\phi)$ across as broad a range of ϕ as possible and for a wide range of system types, thus, rendering Eq. (1) generally predictive. Although a wide range of models for $k(\phi)$ have been proposed, they are often: (1) restricted to a given microstructure type, (2) depend on knowledge of pore network tortuosity, or (3) have empirical adjustable parameters that must be calibrated against experimental or numerical datasets.

Sphere packs, composed of spherical objects of radius R or radius distribution $f(R)$ packed in a volume, represent a standard model system for exploring permeability scaling laws. If we focus on the case for which the intersphere space is the fluid phase and the sphere space is a rigid solid (generally termed the Swiss cheese model system [12,15]), then such systems can be divided into two classes: overlapping (or penetrable) and nonoverlapping (or hard) sphere systems [1,10,12,15–17]. Herein, we use nonoverlapping and hard interchangeably for the latter case. For packs of either hard or overlapping spheres, the accessible range of ϕ is $\phi' < \phi < 1$, where $\phi' > 0$ is a lower limiting value. For packs of hard spheres, ϕ' is given by either a formal maximum packing porosity $\phi' = \phi_m$, such as is the case in regular packs on cubic lattices [8], or a random close-packing (rcp) porosity $\phi' = \phi_{\mathrm{rcp}}$ as is the case for random heterogeneous packs [18,19]. By contrast, for packs of overlapping spheres, ϕ' is given by a percolation threshold porosity $\phi' = \phi_c$. A key difference between these two geometries—hard and overlapping spheres—is then that k has a finite value at $\phi = \phi_m$ or $\phi = \phi_{\mathrm{rcp}}$, whereas $k \to 0$ at $\phi = \phi_c$. This property of ϕ' informs the model formulations for $k(\phi)$ that we will explore here.

For hard spheres there exist expansions of the Stokes equations for flow past a single sphere to account for many spheres at $\phi < 1$ (Refs. [1,8,20]). Sangani and Acrivos [8] present a formulation with the expansion coefficients c_i up to term $i = 30$ for face-centered, body-centered, and simple cubic

*j.vasseur@lmu.de

lattices,

$$k = \frac{2(1-\phi)}{s^2}\left[\sum_{i=0}^{30} c_i \left(\frac{1-\phi}{\phi_m}\right)^{i/3}\right]^{-1}, \tag{2}$$

where s is the specific surface area internal to the pack. We note that in the original contribution, Sangani and Acrivos [8] provide a solution for the fluid drag K, which can be transformed to k (see Vasseur *et al.* [21]). Vasseur *et al.* [21] show that Eq. (2) provides a reasonable description for random packs in the dilute regime $\phi > \phi_{\mathrm{rcp}}$. This result may be surprising given that random packs violate the cubic arrangements on which the model is founded. At intermediate ϕ close to or at ϕ_{rcp}, Eq. (2) breaks down, and the preferred model is the so-called Kozeny-Carman equation [2,7,9,21],

$$k = \frac{\phi^3}{Cs^2}, \tag{3}$$

for which C is an empirical adjustable parameter, and where Eq. (3) with $C = 5$ performs well against data for hard-sphere packs at a wide range of polydispersivity [21]. By contrast, for overlapping sphere packs it might be reasonable to assume that an effective model would account for the percolation threshold porosity ϕ_c below which permeability is zero via a rescaling $\phi - \phi_c$ (Refs. [4,5,17,22]). Martys *et al.* [5] proposed

$$k = \frac{2[1-(\phi-\phi_c)]}{s^2}(\phi-\phi_c)^e, \tag{4}$$

where e is a percolation exponent. For overlapping spheres close to the percolation transition (low ϕ), the theoretical value is $e = 4.4$ (Ref. [15]), close to empirical best-fit exponents of $4.0 < e < 4.2$ (Refs. [4,5]). Monodisperse overlapping spheres form isolated nonpercolating pore spaces at $\phi_c = 0.0301 \pm 0.0003$ (Refs. [16,23,24]).

Regardless of whether the spheres in a pack can overlap with one another or not, the models given by Eqs. (2)–(4) all state that $k \propto s^{-2}$ and the parameter s is a function of the sphere sizes that make up a given sphere pack such that Eqs. (2)–(4) are specific to a given sphere pack of choice. In order to use Eqs. (2)–(4), s must be known from the distribution of sphere sizes. In general, the specific surface area of a pack of spheres is given by

$$s = \frac{3(1-\phi)}{\delta}, \tag{5a}$$

$$s = -\frac{3\,\phi\,\ln(\phi)}{\delta}, \tag{5b}$$

where Eq. (5a) is for hard spheres and Eq. (5b) is for overlapping spheres, $\delta = R$ (monodisperse) or $\delta = \langle R^3\rangle/\langle R^2\rangle$ (polydisperse), and where $\langle R^n\rangle$ is the nth moment of $f(R)$. Using Eq. (5) with δ defined for a given system, we can solve Eqs. (2)–(4) to provide a set of three possible model classes for $k(\phi)$.

As a final step in order to render simulation results or experimental data comparable, regardless of s [and, therefore, regardless of the specific choice of R or $f(R)$], we normalize Eqs. (2)–(4) by a variation of the Stokes permeability k_s,

$$k_s = \frac{2[1-(\phi-\phi_c)]}{s^2}, \tag{6}$$

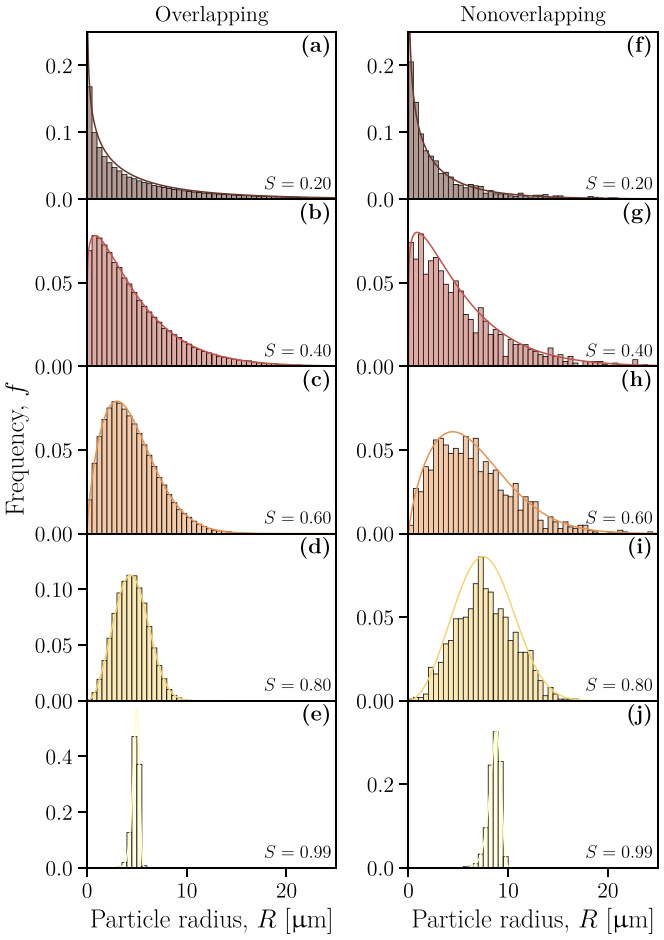

FIG. 1. The distribution of sphere sizes used in the (a)–(e) overlapping sphere domains and (f)–(j) nonoverlapping sphere domains. The discrete histograms represent the measured distributions resulting from the algorithms used, whereas the continuous curves represent the target Weibull distributions.

such that $\bar{k} = k/k_s$. k_s is usually given as $k_s = 2(1-\phi)s^{-2}$, which we note is equivalent to Eq. (6) when $\phi_c = 0$. Defining $\bar{k}$, Eqs. (2)–(4) become

$$\bar{k} = \left[\sum_{i=0}^{30} c_i \left(\frac{1-\phi}{\phi_m}\right)^{i/3}\right]^{-1}, \tag{7a}$$

$$\bar{k} = \frac{\phi^3}{2C(1-\phi)}, \tag{7b}$$

$$\bar{k} = (\phi-\phi_c)^e. \tag{7c}$$

where we take $\phi_c = 0$ in k_s for Eqs. (7a) and (7b), but $\phi_c > 0$ for Eq. (7c). Equation (7) represents a set of model classes that can be compared across overlapping and hard-sphere packs.

Here, the principal aim is to compare predictions of each of the models given by Eq. (7) with data from packs of spheres generated numerically. In order to generate packs of spheres, we use two separate algorithms: (1) a molecular dynamics simulation with sphere growth laws in order to generate hard-sphere packs at a range of ϕ including $\phi \to \phi_{\mathrm{rcp}}$ (Ref. [25]), and (2) a random sphere generation algorithm to produce overlapping sphere packs [16,26]. In each case, we

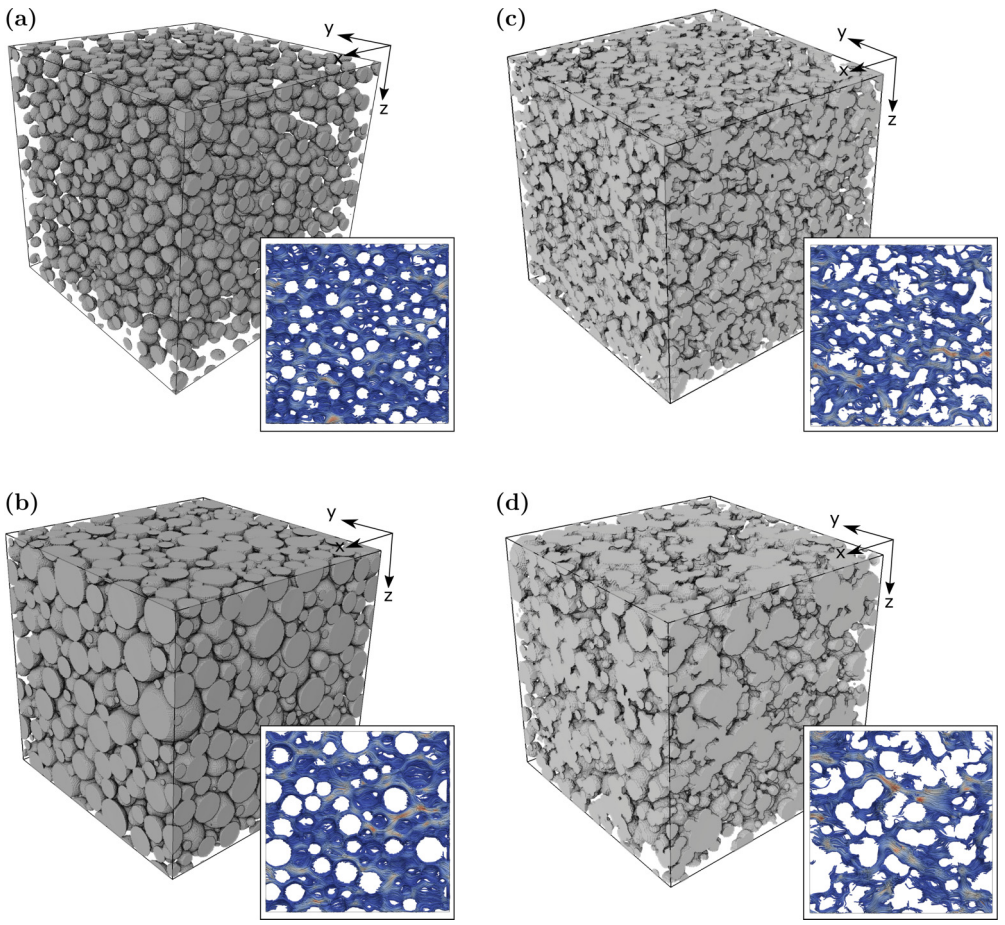

FIG. 2. Some 3D visualizations of examples of the porous microstructures used here for (a) and (b) nonoverlapping spheres, and (c) and (d) overlapping spheres. These domains use monodisperse spheres in (a) and (c) drawn from the radii distributions in Figs. 1(e) and 1(j) or polydisperse spheres in (b) and (d) drawn from the radii distributions in Figs. 1(c) and 1(h). The insets: The steady state velocity vector distribution in a pseudo 2D x-y slice through the full 3D domains showing the relative magnitude of the fluid velocity that arises from a pressure gradient in the x direction.

control the sphere radius distribution $p(R)$ using a Weibull distribution. In the case of the hard-sphere packs, we assign sphere growth rates drawn from a probability distribution $p(r) = \alpha r^{\alpha-1} \exp(-r^{\alpha})$ for which α is a constant shape parameter. At each iteration step, this growth law is applied so that the volume of the spheres increases between r and $r + dr$, and particle-particle collisions are calculated as ϕ_{rcp} is approached. That results in a final distribution $p(R)$ for each given ϕ. In the case of the overlapping sphere packs, we can draw from a Weibull distribution directly $p(R)$. In both cases, domain boundaries are periodic, and the resulting distribution of sphere radii is captured by $S = \langle R \rangle \langle R^2 \rangle / \langle R^3 \rangle$ where $\langle R^n \rangle$ is the nth moment of the distribution $p(R)$. $S \to 1$ represents the monodisperse limit, and low S indicates polydisperse distributions. In Fig. 1, we report the size distributions $f(R)$ used here together with the corresponding Weibull target distributions.

The numerical domains are binarized such that the spheres are given as the solid phase and the intere-sphere volume is given as the fluid phase. For each domain produced, we use a D_3Q_{15} lattice Boltzmann fluid flow simulation algorithm LBflow [27,28] calibrated for predicting the permeability of cubic packs of spheres [17,28]. This algorithm discretizes the fluid phase into lattice fluid nodes and aliquots of fluid mass are iteratively propagated with time t, and collisions are resolved via the lattice Boltzmann approach. Following previous work using LBflow, we apply a pressure gradient of $\nabla P = 0.01$ Pa m^{-1}, a fluid viscosity of $\mu = 1.8205 \times 10^{-5}$ Pa s, and a fluid density $\rho_f = 1.2047$ kg m^{-3}. These conditions ensure that both the Reynolds and Mach numbers of the flow are small throughout [16,17,26] (for our simulations we find $10^{-13} < \text{Re} < 10^{-6}$ and $10^{-16} < \text{Ma} < 10^{-10}$, respectively). The simulation is halted when the average fluid speed does not vary by a factor of more than 10^{-5} twice over 50 iteration steps.

The output of interest of the LBflow algorithm is the distribution of fluid velocity vectors at steady state. We average these and compute an average $\langle u \rangle_j = u_j \phi$, where u_j is the direct average of the speed in a given direction j. In Fig. 2, we show a two-dimensional (2D) slice of the distribution of steady state fluid flow vectors for some example domains. $\langle u \rangle_j$ is then used as an input to Eq. (1) in place of u, to find the permeability in a given direction k_j. We repeat this procedure for each of the three principal directions j. Finally, in order to confirm that our volumes are representative, we apply the approach of Matyka *et al.* [29] and Vasseur *et al.* [21] who apply a normalization of the raw permeability values by the

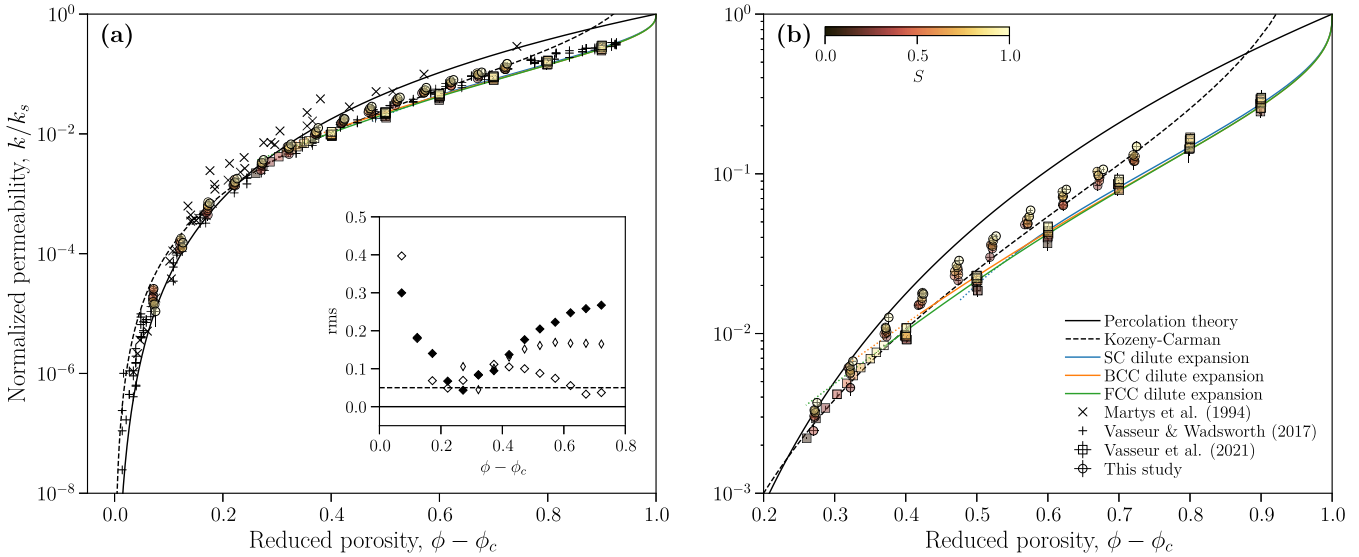

FIG. 3. The result of the simulations and scaling proposed herein cast as k/k_s as a function of the reduced porosity $\phi - \phi_c$. For the dilute expansion results [Eq. (7a)] and for the Kozeny-Carman result [Eq. (7b)], we take $\phi_c = 0$ such that $\phi - \phi_c = \phi$. The hard-sphere results (squares) use $\phi_c = 0$, whereas the overlapping sphere results (circles) use $\phi_c = 0.03$. (a) The full data series. (b) The dilute regime at $\phi - \phi_c > 0.2$. The inset: The result of the rms analysis, showing the data relative to Eq. (7a) (unfilled elongate diamonds), the data relative to Eq. (7b) (unfilled equant diamonds), and the data relative to Eq. (7c) (filled diamonds).

square of a length scale δ and then fit for the dependence on the domain size L using

$$\frac{k}{\delta^2} = k_\infty - k\left(\frac{L}{\delta}\right)^{-2/3}, \tag{8}$$

where k_∞ is the limiting representative permeability at very large L. We use $\delta = \langle R^3\rangle/\langle R^2\rangle = \langle R\rangle/S$ as defined previously and fit each dataset using Eq. (8) to output k_∞ as the permeability of interest. In practice, this means that we present $\bar{k} = k_\infty/k_s$ in the visual reporting of our results here. We note qualitatively that at low ϕ, $k = k_\infty$ for most L used, and so this correction only has a real impact on our results as $\phi \to 1$. Finally, we use a marching cubes algorithm [30,31] to determine s for each domain.

In Fig. 2, we show example three-dimensional (3D) renderings of some example domains of hard and overlapping sphere geometries, created using Avizo^{TM}. In addition to producing new simulations across a wide range of ϕ and S, we compile available simulation results from published sources for which the data necessary to apply the normalization given in Eq. (6) is available. Specifically, we use the monodisperse overlapping sphere simulations and the hard cubic-lattice sphere simulations from Vasseur and Wadsworth [16], and the polydisperse hard-sphere simulations from Vasseur *et al.* [21]. For all overlapping sphere simulation data, we apply $\phi_c = 0.03$, approximately typical for sphere packs [16] and only weakly dependent on sphere polydispersivity [24].

We find that across a wide range of sphere sizes, polydispersivity of sphere radii distributions, and across the random, lattice, hard, and overlapping sphere-pack types, there is a good universal collapse of the data to a single $\bar{k}(\phi - \phi_c)$ trend [Fig. 3(a)]. We also find that there is apparent efficacy of all three of the models given in Eq. (7) when taken in the restricted range of $\phi - \phi_c$. To quantify these ranges, we apply a root mean square statistic rms $= \sqrt{\sum (\bar{k} - \bar{k}')^2/n}$, where $\bar{k}$ is the measured value, $\bar{k}'$ is the model value, and n is the total number of data points at a given ϕ across S. We compute the rms for each ϕ for each model in Eq. (7) separately, resulting in rms$(\phi - \phi_c)$ for each model [Fig. 3(a) inset] where the regions of $\phi - \phi_c$ in which the rms is lower for one model compared with another model indicate overall efficacy of that model for that range of porosity. This approach shows that there appear to be three regimes: (1) a dilute regime at high ϕ where Eq. (7a) or Eq. (7b) is broadly valid; (2) a concentrated regime at low ϕ where Eq. (7b) or Eq. (7c) is valid; and (3) a transitional regime at intermediate ϕ where Eq. (7b) is valid. The range of ϕ for each of these regimes, delimited via the rms, is approximately: (1) $0.40 \lesssim \phi < 1$, (2) $\phi_c < \phi \lesssim 0.30$, and (3) $0.30 \lesssim \phi \lesssim 0.40$.

We note that the collapse to a universal curve is imperfect across all S at $\phi \to \phi_c$ and imperfect between overlapping and hard spheres at $\phi \to 1$. At low ϕ close to ϕ_c, we posit that the imperfect collapse arises because we set ϕ_c to be a constant value for all S, whereas in the few cases where ϕ_c has been determined for $S < 1$, it has been shown to be different from the ϕ_c value at $S = 1$. Specifically, Rintoul [24] found that whereas $\phi_c = 0.0301 \pm 0.0003$ for $S = 1$, $\phi_c = 0.0278 \pm 0.0005$ for a bidisperse distribution of sphere sizes (corresponding to $S = 0.83$). This effect is small, but sufficient to account for the differences observed in our data in $\phi - \phi_c$ space [Fig. 3(a)]. Therefore, we propose that future work should constrain the percolation probability for polydisperse distributions of spheres at $\phi \to 0$. Conversely, at high ϕ the imperfect agreement between overlapping and hard-sphere data is due to the implementation of the rule that $\phi_c = 0.03$ for overlapping spheres, whereas $\phi_c = 0$ for hard spheres. We note that at high ϕ, the meaning of ϕ_c for overlapping spheres is ambiguous and that formally the packs should

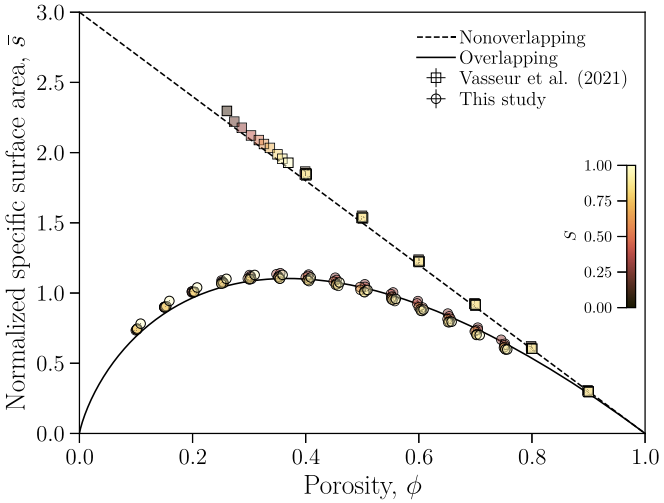

FIG. 4. The normalized specific surface area $\bar{s} = s/\delta$.

be treated as hard-sphere packs with $\phi_c = 0$. In Fig. 3(b) we show this dilute case with $\phi_c = 0$, demonstrating that this, indeed, causes the data to collapse adequately. However, we also note that there is no obvious and simple method by which a continuum of ϕ for overlapping spheres can be associated with $\phi_c > 0$ at low ϕ and associated with $\phi_c = 0$ at high ϕ.

We interpret the three regimes found here in the following manner. First, in the dilute regime, it appears that the permeability is broadly insensitive as to whether the spheres overlap or not and to the details of the arrangements of the spheres; random or lattice arranged. This appears consistent with the observation that the specific surface area s for overlapping and hard spheres converges at high (Fig. 4). Similarly, the detailed arrangement of the spheres is less important when the distance between any two spheres is large (i.e., high ϕ). Second, in the concentrated regime at low ϕ, ϕ is typcially less than the ϕ_{rcp} value, and so hard-sphere packs cannot access this region. However, we note that for low S (highly polydisperse sphere sizes), hard-sphere packs at ϕ_{rcp} diverge toward Eq. (7b) (Fig. 3), and, therefore, polydisperse packs of hard spheres are microstructurally similar to packs of overlapping spheres. Third, the intermediate regime appears to be valid only for intermediate ϕ typically around ϕ_{rcp} values, which may explain the wide use of Eq. (7b) for describing loose packs of particles, such as sediments and soils.

Our collapse of the data across all conditions to a single trend of $\bar{k}(\phi - \phi_c)$ confirms that our scaling of k via Eq. (6) is valid and, therefore, that $k \propto s^{-2}$. This opens up the possibility that packs of nonspherical particles may also collapse to our universal classes [Eq. (7)] if s can be determined or calculated. To test this, we first use existing

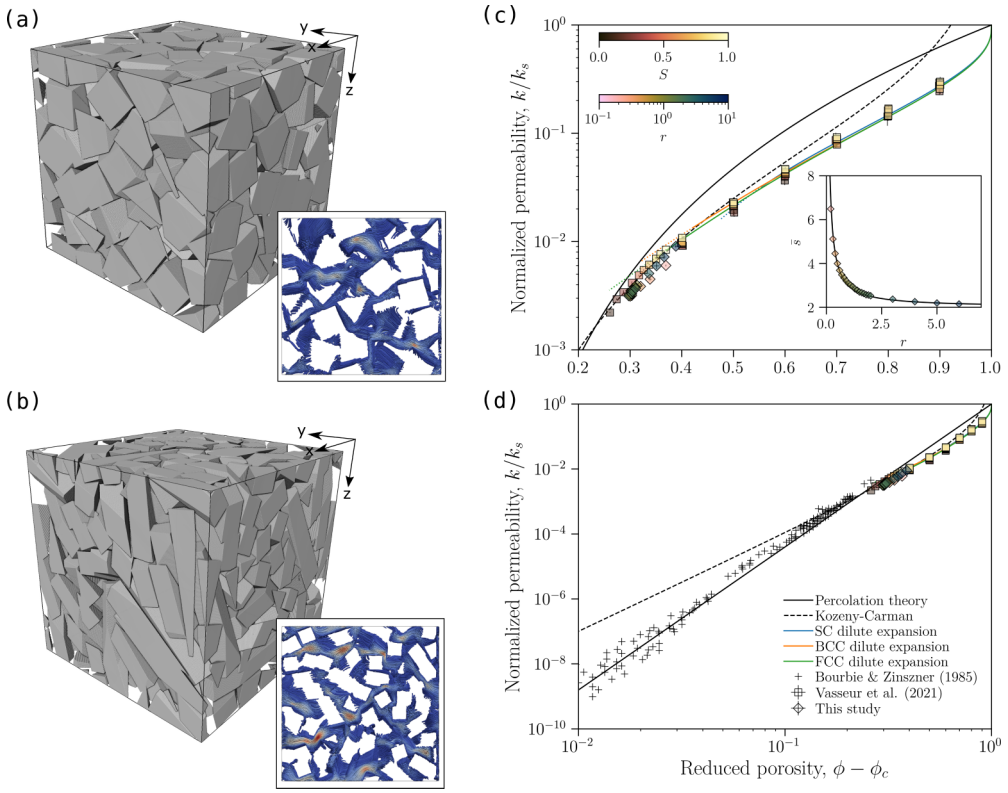

FIG. 5. Extending the models explored here to hard nonsphere and natural rough packs. (a) and (b) Some 3D visualizations of square-ended cuboid packs from Liu *et al.* [32] at aspect ratio (a) $r = 1$ (cubes) and (b) $r = 6$ (prolate needles). In (a) and (b) the inset panels are equivalent to those in Fig. 2 but for the corresponding 3D domain shown here. (c) The result of applying the scaling k/k_s with $\phi_c = 0$ to the permeability data for the cuboid packs (diamonds) over a wide range of r and ϕ close to ϕ_{rcp}. The inset: the specific surface area $\bar{s}$ using the measured s for the cuboid packs, compared with $\bar{s} = 2\phi(1 + r^{-1})$ and $\delta = a$, where a is the side length of the square cuboid end. (d) The full scaling solutions proposed here [as in Fig. 3(a)] with the data for hard-cuboid packs (diamonds) as well as for natural sandstones (crosses) added, extending the solution validity to nonspherical particles, to natural rough particles (sand grains throughout diagenesis), and to very low ϕ close to ϕ_c.

simulations of square-end cuboids at a range of ratios of cuboid length to cuboid breadth provided by Liu *et al.* [32]. We use the same numerical procedure via LBflow and the marching cubes algorithm as described above to output k_∞ and s for each ϕ. Using this information, we can compute $\bar{k}$ and, as with our hard-sphere simulations, we take $\phi_c = 0$. In Fig. 5, we show that these data do, indeed, collapse to the universal $\bar{k}(\phi - \phi_c)$ trend in just the way that our sphere-pack data do.

As a second step in testing the efficacy of our approach for nonspherical particle systems, we use the canonical sandstone dataset produced by Bourbie and Zinszner [33]. These data are for so-called "clean" sandstones (i.e., without pore-filling clays and mineralization) over a wide range of porosity but all produced from the same sedimentary basin environment and so involving the same sand grains as a building block. These data have also been used previously as a test-bed dataset for geological permeability models [4,34]. Sandstones undergo diagenesis, which involves the reduction of porosity below the maximum packing porosity attributable to hard grains alone, and as such sandstones are often in the low-permeability range, compared with the hard-sphere and hard-cuboid numerical domains used herein. We find that the sandstone data used here straddle the porosity ranges spanned by our overlapping and hard particle domains. To plot the data for these sandstones using our normalization, we use a model for the specific surface area interstitial to sand grains during diagenesis [4], which is based on the overlapping sphere model presented here [Eq. (5b)]. Using this, we find that these data collapse to our normalization trend and track from the prediction of Eq. (7a) to that of Eq. (7c), just as the data for overlapping sphere packs do. Along with the data for packs of hard cuboids, this represents an especially hard test of how our scaling approaches perform for nonspherical, heterogeneous, and complex natural cases, extending the utility and universality of our result. However, we note that we have not provided a test of the efficacy of Eq. (7) in describing the permeability of packs of arbitrary shaped particles, including convolute shapes with high convexity.

The data that support the findings of this Letter are available from the corresponding author upon reasonable request.

We are grateful to J. Coumans for interesting discussions associated with permeability and 3D domains of particles. We acknowledge funding provided by the European Research Council (Grant No. ADV 2018 834225–EAVESDROP), the Natural Environment Research Council Grant No. NE/T000430/1, and a Durham Doctoral Scholarship (DDS) to E.B.

J.V. and F.B.W. produced and analyzed the data. All authors conceptualized the study and drafted the paper.

[1] S. Torquato, *Random Heterogeneous Materials: Microstructure and Macroscopic Properties, Vol. 16* (Springer, New York, 2002).

[2] C. F. Berg, Permeability description by characteristic length, tortuosity, constriction and porosity, Transp. Porous Media **103**, 381 (2014).

[3] R. A. Lopes and A. M. Segadães, Microstructure, permeability and mechanical behaviour of ceramic foams, Mater. Sci. Eng. A **209**, 149 (1996).

[4] F. B. Wadsworth, J. Vasseur, B. Scheu, J. E. Kendrick, Y. Lavallée, and D. B. Dingwell, Universal scaling of fluid permeability during volcanic welding and sediment diagenesis, Geology **44**, 219 (2016).

[5] N. S. Martys, S. Torquato, and D. P. Bentz, Universal scaling of fluid permeability for sphere packings, Phys. Rev. E **50**, 403 (1994).

[6] D. L. Johnson, J. Koplik, and R. Dashen, Theory of dynamic permeability and tortuosity in fluid saturated porous media, J. Fluid Mech. **176**, 379 (1987).

[7] M. Röding, Z. Ma, and S. Torquato, Predicting permeability via statistical learning on higher-order microstructural information, Sci. Rep. **10**, 15239 (2020).

[8] A. S. Sangani and A. Acrivos, Slow flow through a periodic array of spheres, Int. J. Multiphase Flow **8**, 343 (1982).

[9] P. C. Carman, Fluid flow through granular beds, AIChE J. **15**, 150 (1937).

[10] S. Torquato and B. Lu, Rigorous bounds on the fluid permeability: Effect of polydispersivity in grain size, Phys. Fluids A Fluid Dyn. **2**, 487 (1990).

[11] A. Nabovati, E. W. Llewellin, and A. C. M. Sousa, A general model for the permeability of fibrous porous media based on fluid flow simulations using the lattice boltzmann method, Compos. Part A Appl. Sci. Manuf. **40**, 860 (2009).

[12] S. Torquato, Flow in random porous media: Mathematical formulation, variational principles, and rigorous bounds, J. Fluid Mech. **206**, 25 (1989).

[13] A. E. Scheidegger, *The Physics of Flow through Porous Media* (Macmillan, New York, 1960) .

[14] S. P. Neuman, Theoretical derivation of darcy's law, Acta Mech. **25**, 153 (1977).

[15] S. Feng, B. I. Halperin, and P. N. Sen, Transport properties of continuum systems near the percolation threshold, Phys. Rev. B **35**, 197 (1987).

[16] J. Vasseur and F. B. Wadsworth, Sphere models for pore geometry and fluid permeability in heterogeneous magmas, Bull. Volcanol. **79**, 77 (2017).

[17] F. B. Wadsworth, J. Vasseur, E. W. Llewellin, K. J. Dobson, M. Colombier, F. W. von Aulock, J. L. Fife, S. Wiesmaier, K.-U. Hess, B. Scheu, Y. Lavallée, and D. B. Dingwell, Topological inversions in coalescing granular media control fluid-flow regimes, Phys. Rev. E **96**, 033113 (2017).

[18] F. Boyer, É. Guazzelli, and O. Pouliquen, Unifying Suspension and Granular Rheology, Phys. Rev. Lett. **107**, 188301 (2011).

[19] S. Torquato, T. M. Truskett, and P. G. Debenedetti, Is Random Close Packing of Spheres Well Defined?, Phys. Rev. Lett. **84**, 2064 (2000).

[20] H. Hasimoto, On the periodic fundamental solutions of the stokes equations and their application to viscous flow past a cubic array of spheres, J. Fluid Mech. **5**, 317 (1959).

[21] J. Vasseur, F. B. Wadsworth, J. P. Coumans, and D. B. Dingwell, Permeability of packs of polydisperse hard spheres, Phys. Rev. E **103**, 062613 (2021).

[22] F. B. Wadsworth, J. Vasseur, E. W. Llewellin, R. J. Brown, H. Tuffen, J. E. Gardner, J. E. Kendrick, Y. Lavallée, K. J. Dobson, M. J. Heap, D. B. Dingwell, K.-U. Hess, J. Schauroth, F. W. von Aulock, A. R. L. Kushnir, and F. Marone, A model for permeability evolution during volcanic welding, J. Volcanol. Geotherm. Res. **409**, 107118 (2021).

[23] J. Kertesz, Percolation of holes between overlapping spheres: Monte carlo calculation of the critical volume fraction, J. Phys. Lett. **42**, 393 (1981).

[24] M. D. Rintoul, Precise determination of the void percolation threshold for two distributions of overlapping spheres, Phys. Rev. E **62**, 68 (2000).

[25] E. Ghossein and M. Lévesque, A fully automated numerical tool for a comprehensive validation of homogenization models and its application to spherical particles reinforced composites, Int. J. Solids Struct. **49**, 1387 (2012).

[26] J. Vasseur, F. B. Wadsworth, and D. B. Dingwell, Permeability of polydisperse magma foam, Geology **48**, 536 (2020).

[27] E. W. Llewellin, LBflow: An extensible lattice boltzmann framework for the simulation of geophysical flows. part i: Theory and implementation, Comput. Geosci. **36**, 115 (2010).

[28] E. W. Llewellin, LBflow: An extensible lattice boltzmann framework for the simulation of geophysical flows. part ii: Usage and validation, Comput. Geosci. **36**, 123 (2010).

[29] M. Matyka, Z. Koza, J. Gołembiewski, M. Kostur, and M. Januszewski, Anisotropy of flow in stochastically generated porous media, Phys. Rev. E **88**, 023018 (2013).

[30] W. E. Lorensen and H. E. Cline, Marching cubes: A high resolution 3d surface construction algorithm., Comput. Graph. **21**, 163 (1987).

[31] T. Lewiner, H. Lopes, A. Vieira, and G. Tavares, Efficient implementation of marching cubes' cases with topological guarantees, J. Graph. Tools **8**, 1 (2003).

[32] L. Liu, Z. Li, Y. Jiao, and S. Li, Maximally dense random packings of cubes and cuboids via a novel inverse packing method, Soft Matter **13**, 748 (2017).

[33] T. Bourbie and B. Zinszner, Hydraulic and acoustic properties as a function of porosity in fontainebleau sandstone, J. Geophys. Res.: Solid Earth **90**, 11524 (1985).

[34] P. E. Øren and S. Bakke, Process based reconstruction of sandstones and prediction of transport properties, Transp. Porous Media **46**, 311 (2002).